American Journal of Condensed Matter Physics 2025, 14(1): 8-17
DOI: 10.5923/j.ajcmp.20251401.02

Effects of Glutathione Concentration Used as a Capping Agent on the Structural, Optical, and Photoluminescence Properties of Fe: ZnO NPs

Ayabei Shadrack[1], John Njagi[1], Jatani Ungula[2], Sharon Kiprotich[1,*]

[1]Department of Physical and Biological Sciences, Murang'a University of Technology, Murang'a, Kenya
[2]Department of Pure and Applied Sciences, Kenya Methodist University, Meru, Kenya

Abstract Glutathione (GSH) capped Iron-doped zinc oxide nanoparticles (GSH-Fe: ZnO NPs)at varying GSH concentrations (0.002, 0.004, 0.006, 0.008, 0.01, 0.012, 0.014M) were successfully synthesized through sol-gel route to study their effects on the structural, optical,and morphological properties. Characterization was carried out using X-ray diffractometer (XRD), photoluminescence (PL) spectroscopy, and Ultraviolet-Visible spectrometer (UV- Vis). While Fe: ZnO NPs have interesting optical and photoluminescence properties, their usage in bio-imaging are still limited by surface imperfections and poor biocompatibility. More surface functionalization approaches, such as biomolecule-based capping, are needed to improve their performance and biocompatibility.XRD confirmed the retention hexagonal wurtzite structure and successful incorporationof Fe into the ZnO lattice. Optical analysis showed systematic absorbance modulation, a blue shift, and reduced optical bandgap (3.0 eV) at 0.008 M GSH capping. The PL analysis revealed that GSH capping enhances emission intensitybecause GSH reduces non-radiative recombination and facilitates light emission. The PL spectra deconvolution reveals the presence of near-band emissions (NBE) and deep-level emissions (DLE). FTIR analysis revealed that glutathione capping to the Fe-doped ZnO NPs occurred through N–H, C=O, and COO^- bonds. This result not only addresses the existing knowledge gap on surface functionalization but also establishes a foundation for future nanomedical applications of these NPs.

Keywords Capping agent, Doping, Glutathione, Bioimaging, Sol gel, GSH-Fe: ZnO NPs

1. Introduction

Zinc oxide (ZnO) nanoparticles have attracted considerable attention in nanotechnology because of their peculiar optical, electronic, and chemical attributes. Their wide bandgap of 3.37 eV and high exciton binding energy of 60 meV make them useful for various applications such as optoelectronics, sensors, and biomedical imaging [1]. However, pure ZnO nanoparticles tend to have such limitations as an excessive rate of electron-hole recombination and a lack of visible light absorption, which may limit their effectiveness in some applications [2]. Studies have shownthat these challenges can be addressed through doping ZnO with metals, such as iron (Fe) [3]. Iron introduces additional levels of energies in the band structure of ZnO, which increases the absorption of visible light and improves the magnetic characteristics desirable for applications such as magnetic resonance imaging (MRI) and target delivery of drugs [4]. It has been found that Fe: ZnO NPs present better photocatalytic activity and magnetic reactivity, which qualifies them as promising materials for multifunctional biomedical applications [4]. Surface modification of nanoparticles is yet another important factor that affects stability, dispersibility, and interactions with biological systems [5]. Capping agents, which are molecules that bind on the surface of nanoparticles, are extremely important as they help in controlling particle growth and also in inhibiting particles from agglomeration as well as serving as reactive functional groups for further conjugation [6]. Among various capping agents tested, glutathione (GSH) stands out since it is a tripeptide composed of glutamine, cysteine, and glycine, because of its biocompatibility, antioxidant properties, and the ability to bind metal ions through its thiol group [7]. GSH-capped nanoparticles present improved stability and lower toxicity, therefore being suitable for biomedical applications [8]. Although there are several benefits associated with Fe doping and GSH capping individually, to date, there are limited reports on the combined effects of varying GSH concentrations upon the properties of Fe: ZnO NPs. This interplay is very significant as the level of GSH

* Corresponding author:
Skiprotich@mut.ac.ke (Sharon Kiprotich)
Received: Jun. 7, 2025; Accepted: Jul. 3, 2025; Published: Jul. 25, 2025
Published online at http://journal.sapub.org/ajcmp

can modify the size, morphology, surface charge, and optical characteristics of the nanoparticles, which have an impact on their performance in bioimaging applications [9]. The role of glutathione (GSH) as a capping agent onpure ZnO NPs and doped ZnO NPs has been the subject of numerous investigations, although limited work has been carried out regarding the latter [10] stated that GSH-capped tin-doped ZnO nanoparticles had the optical characteristics modified because of a blue-shift absorption process; however, their research focused on antibacterial activity with no focus on structure and morphology. Another study by [11] proved that GSH concentration affected the formation of star-shaped ZnO nanoparticles, but they did not quantify the effect of GSH related to the crystallinity or detailed morphology. Conversely, [12] synthesized Fe-doped ZnO NPs with the use of bio-ingredients, showing their structural and optical properties, though GSH was not involved in their synthesis pathway, excluding it as a capping agent. According to these studies, there is a definite gap evident in the composite effects of iron doping and varying concentrations of GSH in Fe: ZnO NPs characterizations in terms of structure and morphology have not been thoroughly investigated, especially regarding particle growth, crystallinity, and shape control mechanisms. This work is intended to fill that gap.

There are a variety of synthesis methods that have been used to synthesize ZnO nanoparticles, ranging from hydrothermal, sol-gel, to microwave-assistedtechniques, and the combustion method. However, the sol-gel method is advantageousbecause it offerslow processing temperatures, it is relatively cost-effective, and it hasthe ability to precisely adjust the composition and morphology of the nanoparticles [13]. Sol gel involves the transformation of a system from liquid "sol" to solid "gel" phase, leading to even doping and surface modification [13]. In this study, the aim is to fill the research gap that currently exists by systematically experimenting on the structural, optical, and morphological properties of Fe: ZnO NPs prepared using the sol-gel process, and varying GSH concentrations as capping agents. By clarifying the dependencies of GSH concentration and characteristics of nanoparticles, this work will possibly maximize the synthesis conditions for future imaging purposes, working towards the creation of multifunctional NPs for use in biomedicine.

2. Methodology

Chemicals

Zinc acetate dihydrate Zn $(CH_3COO)_2\cdot \bullet H_2O$ of purity 99.9%, as a metal precursor, Iron (III) nitrate nanohydrate Fe $(NO_3)_3\cdot 9H_2O$ of 98% purity, as the source of iron, Ethanol C_2H_5OH of 99.9% purity as a solvent for the precursor, Diethanolamine (DEA) $C_4H_{11}NO_2$ of 99.3% purity as a complexing agent, Deionized water (DI) (H_2O), Glutathione (GSH) as the capping agent, all supplied by Sigma Aldrich. All reagents were of analytical grade and were used directly without any special treatment.

Experimental procedure

Sol-gel technique was adopted from [14] to synthesize Fe: ZnO NPs by adding 4.4g of Zn $(CH_3COO)_2\cdot(H_2O)$ to 100 mL of ethanol in a clean beaker on a magnetic stirrer at room temperature. DEA (2 mL) was added after 15 minutes, and stirring continued until a transparent solution was formed. 0.45% Fe was added, and stirring was continued for another 30 minutes. 0.002M GSH was added and allowed to dissolve for 15 minutes. 1.6M NaOH was added dropwise using a burette to adjust the pH to 11 with the aid of a pH meter. The contents were then transferred to a hot magnetic stirrer set at 65℃, and heating took place for 2hrs where a gel-like solution was formed. The solution was covered in a clean foil and left to age overnight. The gel was rinsed several times with DI water before drying in an oven at 100℃ for 2hr to eliminate residual solvents and finally annealed in a muffle furnace at 500℃ for 1 hour. The sample was ground into fine GSH-capped Fe: ZnO NPs and kept in a sample holder for further analysis. The procedure was repeated for other GSH concentrations (0.004, 0.006, 0.008……...0.014M).

Characterization Techniques

X-ray diffraction analysis was done using an X-ray diffractometer model ARL EQUINOX 100 with Cu-Kα radiation (λ=1.5406Å) to determine the phase purity, crystalline structure, and crystallite size of synthesized GSH-capped Fe: ZnO NPs. Photoluminescence spectroscopy (PL) model Infitek SPLF97 Fluorescence spectrometer was used to determine the optical emission properties and defect states of the synthesized GSH-capped Fe: ZnO NPs. The measurements were performed at room temperature with an excitation wavelength of 300nm. An Ultra Visible spectrophotometer was used to obtain the absorbance spectra at room temperature at the wavelength range of (200-800 nm).

XRD analysis

The structural and optical properties of sol-gel synthesized Fe-doped ZnO (Fe:ZnO) nanoparticles capped with various concentrations of glutathione (GSH) were examined using X-ray diffraction (XRD). Figure 1 shows diffraction patterns which substantiate the facts that all samples, irrespective of the GSH concentration, exhibited the hexagonal wurtzite phase of ZnO according to (JCPDS card no. 01-070-8072), no extra phase, such as iron oxide or GSH derivatives, were observed. This indicates successful incorporation of Fe without phase segregation and non-destructive performance of GSH as a capping agent.

The summarized data in Table 1 show that the most intense diffraction peak observed at approximately 38° corresponds to the (101) plane, a dominant feature in the hexagonal wurtzite structure of ZnO. Notably, the 2θ position of this peak exhibited a gradual leftward shift from 38.422° in uncapped Fe:ZnO to 38.065° at 0.014 M GSH concentration, indicating subtle lattice expansion. Such peak shifts usuallyemerge from internal strain or the substitution of host Zn^{2+} ions (0.74 Å) with smaller Fe^{3+} ions (0.64 Å), which cause slight distortions in the ZnO lattice. However,

GSH molecules interacting with nanoparticle surfaces may induce additional tensile strain via steric hindrance or surface passivation, thereby expanding the lattice constants. These observations are consistent with findings of [15], who attributed 2θ peak shifts to strain effects introduced by both dopant ions and organic capping agents.

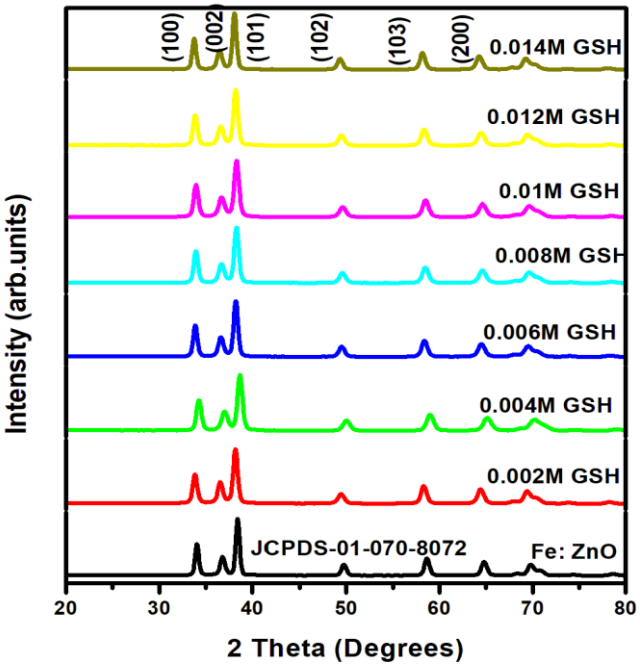

Figure 1. XRD pattern for Fe: ZnO NPs and GSH-capped Fe: ZnO NPs at different GSH concentrations

The crystallite size, interplanar d spacing were calculated using the Debye-Scherrer formula and Bragg's equation, respectively. The results obtained are summarized in Tables 1 and 2. Equation 1 gives Bragg's equation [16], Equation 2 gives the Debye-Scherrer formula [17].

$$n\lambda = 2d \sin\theta \quad (1)$$

Where n represents the order of diffraction (n=1), λ is the wavelength of the incident rays, d is the interplanar spacing between crystal planes, and θ is Bragg's angle, which is half of the 2θ.

$$D = \frac{0.9\lambda}{\beta \cos\theta} \quad (2)$$

Where D is the crystallite size in (nm), λ is the wavelength 1.5406Å (Cu Kα radiation) of X-rays (1.5406Å), β is the full width at half maximum (FWHM) of the peak in radians, and θ is the Bragg angle.

The calculated average crystallite size (D) from the position of the (101) peak, the most intense, and based on the Scherrer equation, followed a nonlinear behavior with an increase in GSH concentration. Thus, the average crystallite size for the uncapped Fe:ZnO was characterized to be 21.51 nm, which reduced to a minimum of 15.9 nm for a GSH concentration of 0.008M before increasing again to 21.9 nm at 0.014 M. This reduction in the crystallite size up to 0.008 M GSH could be attributed to the high interaction between thiol and amine groups of GSH with Zn^{2+} ions on the nanoparticle surface that inhibits the growth of these crystals by sterically preventing the agglomeration process [18]. However, beyond 0.008M, excessive GSH may lead to increased capping layer thickness or cause the particles to clump together, effectively reducing the ability to further restrain grain size growth [19]. These observations match the results obtained by [20], who mentioned that GSH controls the growth of ZnO nanocrystals up to a certain extent, beyond which steric hindrance turns the control against the crystal growth. Moreover, the XRD patterns show that as the concentration of GSH increases, the crystallite size decreases gradually. Larger full width at half maximum FWHM at maximum intensity signifies smaller crystallite size and greater microstrains. For instance, the FWHM of the (101) peak, which was recorded as 0.40882° for the uncapped, was raised to 0.53444° at 0.004 M GSH and then gradually declined with the continuous increase of the GSH concentration. The trend towards higher values of surface energy and strain as seen at lower GSH concentrations due to smaller crystallite sizes, which are stabilized at higher GSH concentrations.

Numerically, the microstrain (ε) and dislocation density (δ) were also determined to analyze various internal defects and distortions resulting from an interaction with GSH. The strain was calculated using the Williamson-Hall method, shown by equation 3 and 4 [21].

$$\varepsilon = \frac{\beta}{4 \tan\theta} \quad (3)$$

Where ε represents the microstrain, β is the FWHM in radians, and θ is the diffraction angle of the most intense peak (101). And the dislocation was calculated using the Williamson-Smallman equation below

$$\delta = \frac{1}{D^2} \quad (4)$$

Where δ is the dislocation density in nm^{-2}, and D is the crystallite size in (nm).

The values of strain varied from 0.0051 to 0.0066, and dislocation density reached its highest 0.004 M GSH (4.03 x 10^{-5} nm^{-2}) at a smaller size of crystallite size. This is logical as the particles that are smaller in size typically possess greater strain and dislocation density due to the larger surface area to volume ratio. The strain and defect density increases at lower GSH concentrations also relate optically with these phenomena, e.g., with bandgap narrowing and enhanced photoluminescence, because lattice distortions may form shallow donor or acceptor levels near the conduction or valence bands [22]. Therefore, structural disorder due to the presence of doping of Fe^{3+} and GSH capping is essential to determine the optical properties of the nanoparticles. Similar trends of crystallite size, strain, and defect density have been observed in Fe-doped ZnO NPs by [23] where both Fe addition and surface capping affect the micro-strain in tune with the particle size.

Table 1. Showing the crystallite sizes, microstrain, and dislocation densities of synthesized GSH-capped Fe: ZnO NPs

	Glutathione (GSH)	Fe: ZnO	0.002M	0.004M	0.006M	0.008M	0.01M	0.012M	0.014M
2θ (Degrees)	100	34.05	33.84	34.26	33.87	33.94	33.95	33.86	33.73
	002	36.80	36.55	37.03	36.63	36.70	36.71	36.60	36.47
	101	38.42	38.18	38.66	38.22	38.29	38.30	38.20	38.06
β (Degrees)	100	0.4019	0.4897	0.5226	0.4506	0.4669	0.4950	0.4825	0.4268
	002	0.5103	0.5031	0.6803	0.5483	0.5903	0.6633	0.5956	0.5480
	101	0.4688	0.4395	0.4544	0.4990	0.5381	0.4745	0.4419	0.4159
Peak Intensity	100	4322.0	2705.6	2908.3	3846.8	3681.0	2983.6	3078.2	3825.6
	002	2427.5	1830.7	1696.4	2202.4	2018.3	1689.0	1784.1	2225.6
	101	7728.8	5172.5	5302.1	68555.8	6427.4	5241.2	0.48192	6946.2
D (nm)	100	20.66	21.95	21.96	16.14	14.63	18.91	20.36	23.50
	002	22.31	22.01	20.31	18.26	15.17	19.61	20.04	20.26
	101	21.56	22.04	19.68	20.20	17.90	19.20	20.29	21.94
Average D (nm)		21.51	22.00	20.65	18.20	15.90	19.24	20.23	21.90
δ		0.0000236	0.0000339	0.0000403	0.0000311	0.0000337	0.0000374	0.0000329	0.0000269
ε		0.005119	0.006172	0.006648	0.005906	0.006135	0.006464	0.006071	0.005514

Table 2. Showing lattice parameters and average d spacing of GSH-capped Fe: ZnO NPs

Glutathione (GSH) concentration(M)	2θ (Degrees)	'a'	'c'	Average d spacing (Å)
Fe: ZnO	38.422	1.7834	2.8570	2.3409
0.002	38.180	1.7943	2.8745	2.3552
0.004	36.661	1.7728	2.8400	2.3270
0.006	38.221	1.7924	2.8715	2.3528
0.008	38.294	1.7891	2.8662	2.3485
0.01	38.307	1.7885	2.8653	2.3477
0.012	38.207	1.7931	2.8725	2.3536
0.014	38.065	1.7995	2.8828	2.3621

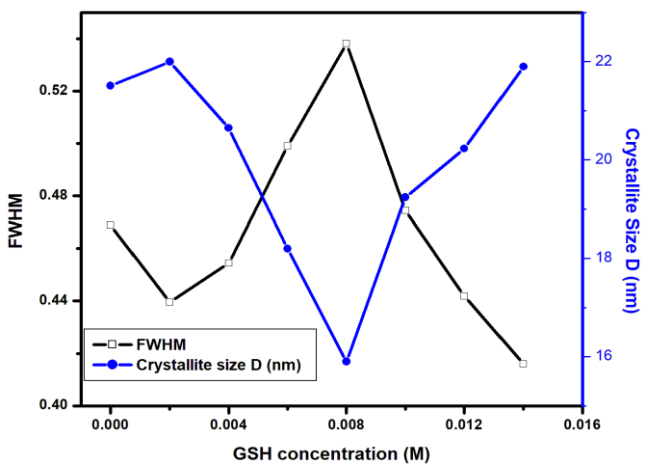

Figure 2. Variation of FWHM and Crystallite size at different GSH capping concentrations

An increase observed in average interplanar d-spacing values, summarized in Table 2 based on Bragg's Law, exhibits the slight spacing increases with the rise of the GSH concentrations. The d-spacing rose from 2.3409 Å for uncapped Fe: ZnO to 2.3621 Å at 0.014 M GSH, which again suggests that GSH has a lattice-expanding effect that could be attributed to GSH adsorption on the ZnO surface or changes in the charge distribution at the boundary of the lattice [24]. The results also demonstrate moderate changes in lattice parameters, a and c, as well, with the elevation of GSH concentration. Such differences indicate that GSH capping causes changes to the ZnO lattice structure, probably by surface interactions, e.g. hydrogen bonding or coordination of -SH and -NH_2 groups with surface Zn^{2+} sites. These forces can induce internal stress or surface-induced relaxation, creating small lattice strains or expansion, as shown in the noted changes of interplanar spacing.

Photoluminescence Analysis

Figure 3 shows the PL spectra of Fe: ZnO and GSH-capped Fe: ZnO NPs at an excitation wavelength of 300nm, recorded at room temperature at an emission range of 250nm to 800nm. This analysis aimed to assess the influence of different concentrations of GSH capping on the deep-level effect emissions and band edge emission of Fe: ZnO and GSH-capped Fe: ZnO NPs.

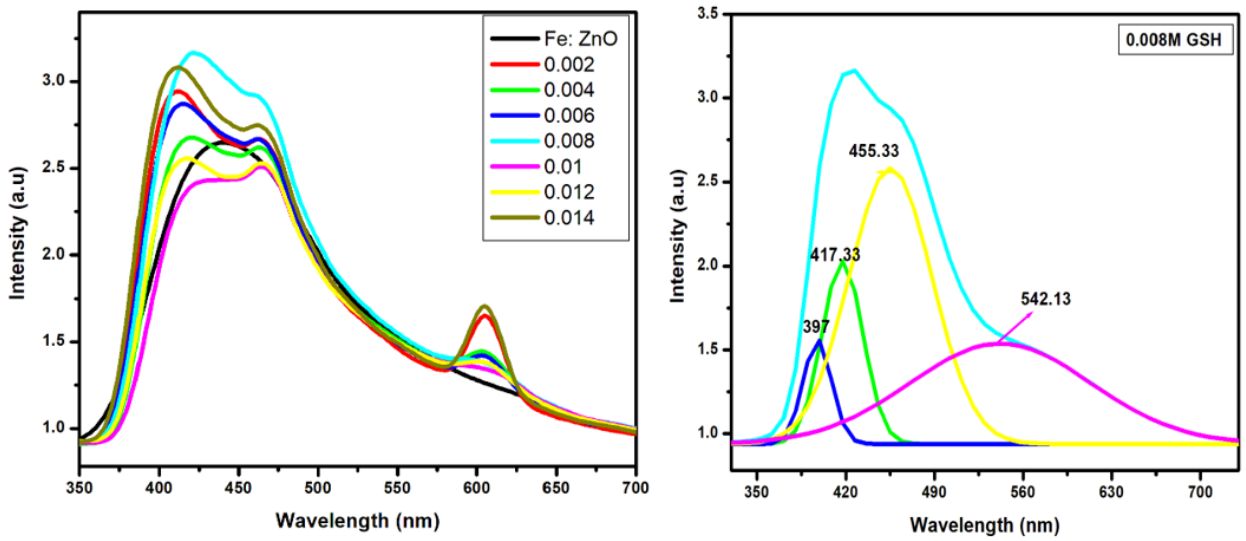

(a) **(b)**

Figure 3. **(a)** PL spectra of synthesized GSH-capped Fe: ZnO NPs at varying GSH concentrations and PL deconvolution at 0.008M GSH capping **(b)**

PL spectra of Fe: ZnO NPs and glutathione (GSH) capped Fe: ZnO at different GSH concentrations (0.002 M to 0.014 M)display a characteristic UV emission centered at 390–470 nm, originating from NBE excitonic recombination, and a weak emission peak in the visible region around 540–600 nm, originating from defect-related features. The Fe:ZnO sample exhibits a broad UV emission peak at 454.5 nm and a relatively low PL intensity (1.525 a.u). This demonstrates that Fe doping enables a transition to excitonic radiative recombination but also suggests that Fe ions may lead to non-radiative recombination. Adding GSH initially results in an improvement in the PL intensity, steadily increasing up to 0.008 M (1.9973 a.u.), followed by a decline for higher concentrations as surface passivation becomes more pronounced. GSH, a thiol-containing tripeptide, serves as a surface passivating agent by interacting with its SH and carboxyl groups to reduce the density of surface defects [7]. The capping action minimizes undesirable non-radiative recombination channels while promoting radiative processes within the material, leading to an improvement in the PL intensity at concentrations below 0.008 M. The decrease in PL at higher GSH concentrations suggests that a thick capping film may restrict the mobility of surface carriers or cause energy migration and non-radiative decay [7].

PL deconvolution spectra of 0.008 M GSH-capped Fe:ZnO show distinct peaks at 397 nm, 417 nm, 455 nm, and 542 nm that correspond to different recombination mechanisms. The emission peaks at 397 and 417 nm are generally attributed to excitonic recombination and shallow donor defects such as zinc interstitials, whereas the green-yellow emission observed at 542 nm can be linked to deep-level emissions originating from oxygen vacancies and interstitials [25]. The redistribution of the NBE peak with different GSH concentrations could be a consequence of changes in surface electronic properties or the presence of weakly-bound electron structures [26]. This behavior has been observed in previous studies focused on varying the surface modification of ZnO NPs. Recently, [27] found that the PL intensity of ZnO nanocrystals could be increased after treatment with glutathione. They explained that this was likely due to the interaction between glutathione and defect sites, thereby improving charge carrier recombination. Moreover, Fe impurities present in the ZnO lattice lead to the formation of states below the conduction band, contributing to efficient carrier localization and ultimately, regulating luminescence behavior [28].

Table 3. Showing the emission wavelengths and PL intensities of GSH-capped Fe: ZnO NPs at different GSH concentrations

GSH Concentration (M)	Emission Wavelength (nm)	PL Intensity (a.u)
Fe: ZnO	454.51	1.5250
0.002	441.96	1.6142
0.004	450.77	1.5386
0.006	445.67	1.7170
0.008	446.34	1.9973
0.010	456.47	1.3771
0.012	451.28	1.4207
0.014	440.33	1.7366

Optical Analysis

The absorption spectra and Tauc plots for both Fe:ZnO and GSH-capped Fe:ZnO NPs were examined using UV-Vis spectroscopy. Figure 4 shows the absorbance spectra demonstrating a strong absorption in the UV part of the UV-Vis range, and a part of this absorption is seen in the visible spectrum, especially for samples capped with GSH. Among the samples tested, 0.008 M GSH capped Fe: ZnO exhibits the highest absorbance across all wavelengths, showing more defects on its surface and better binding of GSH to the NPs. This increased absorbance can be attributed to ideal surface modification at 0.008 M GSH, where GSH not only gives substantive coverage of the surface but also

does not form a thick shield that isolates the surface [29]. The capping enhances the dispersion of nanoparticles and prevents agglomeration, andenhances the effective surface area exposed to light. Also, surface states formed through the coordination of Zn^{2+} and GSH enable sub-bandgap electronic transitions, which spread the absorption into the visible spectrum. The effects heightened and broadened by the combination lead to enhanced and broader light absorption as reported in other GSH-decorated metal oxide systems as well [29]. Such behavior has been reported by [30], who observed the same rise in absorbance for ZnO cysteine-functionalized NPs and attributed it to surface binding and the creation of more defects on their surfaces. In addition, the same behavior in absorbance has been found by [31], where GSH-modified ZnO quantum dots demonstrated a broadening and strengthening in absorption caused by the transfer of electrons from the ligand to the metal and the appearance of new energy states below the bandgap.

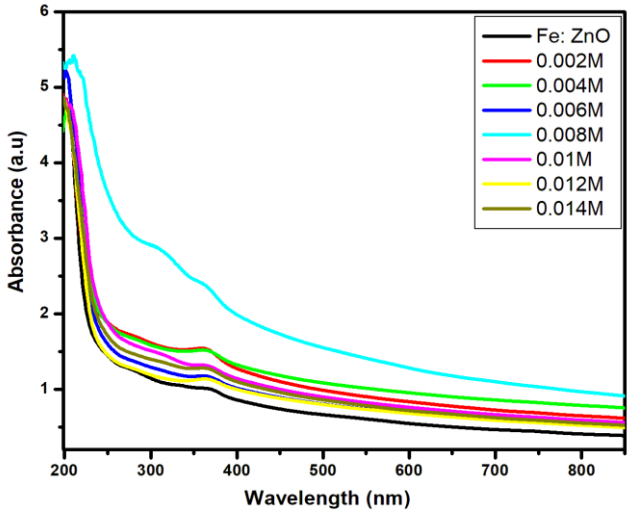

Figure 4. Absorbance spectra of synthesized GSH-capped Fe: ZnO NPs at different GSH concentrations

To calculate the optical bandgap (E_g) quantitatively, Tauc plots were constructed, by use of Tauc relation. Equation 5 gives the Tauc relation [32].

$$(\alpha h\nu)^n = A(h\nu - E_g) \quad (5)$$

Where α is the absorption coefficient, $h\nu$ is the photon energy, E_g is the optical bandgap, A is a constant, while n depends on the number of electronic transitions. $n=\frac{1}{2}$ for direct allowed transitions, while n = 2 for indirect allowed transitions. Since ZnO is a direct bandgap semiconductor, $n=\frac{1}{2}$ was used. The Tauc plot was obtained by plotting $(\alpha h\nu)^2$ against photon energy ($h\nu$), and the optical band gap was obtained by extrapolating the linear portion of the curve to the x-axis where $(\alpha h\nu)^2 = 0$. Figure 5 shows the optical band gaps obtained through extrapolation.

From the extrapolation in Figure 5, the bandgap of Fe:ZnO NPs, measured at 4.14 eV, is slightly blue-shifted from that of the standard value of pure ZnO (3.37 eV). This change is attributed to the Burstein–Moss effect and Fe^{3+} atoms being substituted for Zn^{2+} in the material, which introduces localized states within the band structure [33]. When GSH is introduced, the bandgap swiftly drops from the original value to 0.008 M (3.0 eV), then changes in a non-consistent pattern. As the concentration of GSH capping increases, the bandgap is observed to narrow. This indicates better passivation of surface defects and less chance of recombination, which enables optical transitions below the semiconductor bandgap [34]. The GSH molecule, with its –SH and $–NH_2$ groups, can coordinate with the Zn^{2+} ions on the surface of the nanoparticle and modify its potential, which leads to localized states within the gap around the Fe: ZnO NPs [35]. This coordination is brought about by the electron-donating groups of GSH both in the form of a GSH-SH (thiol), and also GSH-NH_2 (amine) groups. These functional groups carry isolated electron pairs that can donate to the empty orbitals of the Zn^{2+} ions to generate coordinate covalent bonds. These contacts are dynamically favorable, and the result is a complexation of the surfaces, a stabilizing effect on the nanoparticle structure, as well as an effect on the immediate electronic environment. Zn ligand binding through similar mechanisms has been observed on thiol and amine functionalized metal oxides [36]. Similarly, the sharpest change in redshift and maximum bandgap narrowing (3.0 eV) was recorded at 0.008 M GSH, which is consistent with the strongest light emitted as seen in PL analysis. This suggests that 0.008 M is the optimal capping concentration to increase light absorption and allow switching between defect states that are important for bioimaging fluorescence. Similar findings have been reported by [7] found that GSH-capped ZnO quantum dots had a narrow band gap and stronger photoluminescence at optimum capping. However, when 0.008 M, the bandgap increases again (4.12 eV at 0.012 M) for the same reason as before: the GSH molecules cover the surface of the nanoparticles so much that an insulating layer forms, limiting the quantum confinement effect [37]. This also shows a link between the reduced PL brightness at high GSH levels.

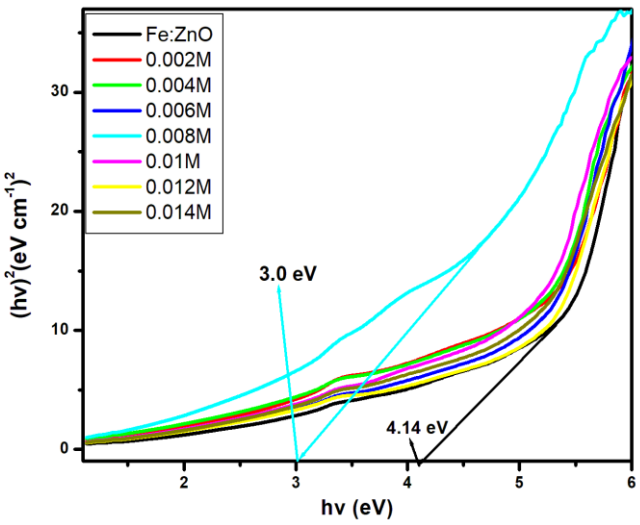

Figure 5. Tauc plotand band gap extrapolation of synthesized GSH-capped Fe: ZnO NPs

Table 4. Showing extrapolated band gap values at each GSH concentration

GSH capping concentration (M)	Band gaps (eV)
Fe: ZnO	4.14
0.002	3.92
0.004	3.85
0.006	3.77
0.008	3.0
0.01	3.82
0.012	4.12
0.014	4.0

The GSH coating allows the Fe:ZnO NPs band gap to be lowered from 4.14 eV to 3.0 eV, supporting their use in customized bioimaging. The reduction in band gap due to an increase in GSH concentration, especially at 0.008 M, may be ascribed to the interaction between GSH and surface states on the nanoparticles. The Zn^{2+} binds to -SH and -NH_2, and on the surface, it forms surface complexes that create new energy levels, commonly shallow defect states, in the band structure. These mid-gap states allow electronic transitions to be made with less energy, lowering the optimal band gap. Moreover, there is a surface passivation by GSH, which lowers non-radiative recombination centers, facilitating the further electronic delocalization and pushing the absorption edge to long-wavelengths [38].

A smaller bandgap allows visible light to be absorbed, so excitation can be performed with low-energy sources that are useful for live imaging [39]. The ability of GSH as a capping agent to improve both the solubility and compatibility of NPs, as well as impact the way the material absorbs light, makes it an effective choice for optoelectronic and biomedical devices [40].

FTIR Analysis

The surface chemistry and molecular effects of Glutathione (GSH) capped Fe: ZnO NPs at different GSH concentrations were studied using FT-IR spectroscopy. Prominent vibrations observed in the FTIR spectra in Figure 6 at 400- 4000 cm^{-1} are attributed to Zn–O and Fe–O interactions, GSH features, and surface hydroxylation are key elements in maintaining nanoparticle stability and can be functionalized for bioimaging purposes.

There is a noticeable absorption band at 617 cm^{-1} from Zn–O and Fe–O likely forms part of the weaker shoulders in this region [41]. This band was found in all parts of the spectra and showed noticeable modulation as GSH concentration increased, indicating that capping influences the local bonding environment within the lattice. The peak does not change with GSH concentration, confirming that the main structure of ZnO is maintained post-functionalization. After adding glutathione, the spectra showed a rise in new peaks, mainly in the range of 1500–1700 cm^{-1}. The peaks formed are a result of certain vibrational modes brought about by an interaction between glutathione and the nanoparticle surface. The band around 1667cm^{-1} corresponds to stretching C=O (amide I band), and the band around 1607cm^{-1} can be related to bending of N-H(amide II band) in the glutathione molecule. Their presence indicates that the occurrence of glutathione is not just a physical adsorption but a chemical coordination by the primary amine and carboxylate groups. This coordination modifies the local vibrational context, giving rise to newly or highly-amplified IR-active modes across the 1500-1700 cm^{-1} range, is consistent with previous findings on biomolecule-functionalized metal oxides [42].

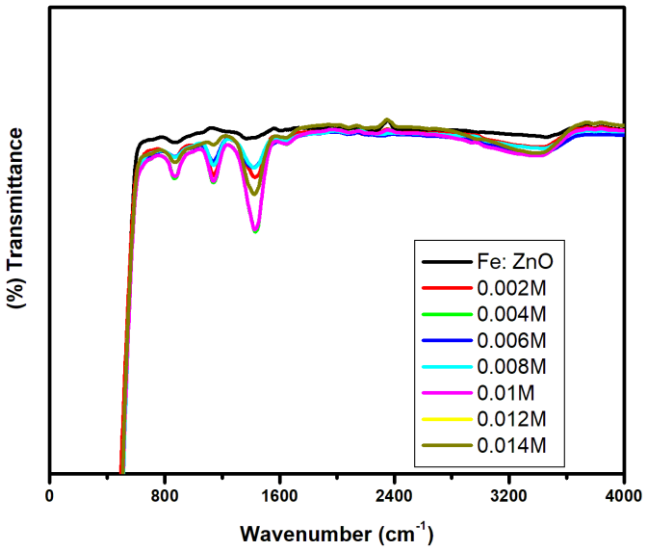

Figure 6. FTIR spectra of GSH-capped Fe: ZnO NPs at different capping concentrations

In particular, absorbance was seen at 1667 cm^{-1} and 1607 cm^{-1}, representing the C=O vibration from glutathione's carboxyl group and the N–H vibration of the primary amines [43]. These observations prove that glutathione has been successfully attached to Fe: ZnO NPs. As the GSH concentration rises, the bio-functionalized layer becomes thicker and the bonds between GSH and the nanoparticle surface become stronger. A characteristic peak at 1563 cm^{-1} signals asymmetric stretching of COO^- groups, showing that the carboxylic acid group has been deprotonated and can take part in either binding to metals or covalent bonds on the surface [44]. Also, O–H stretching features appear in all spectra from 3200 to 3500 cm^{-1} and are related to hydroxyl groups and hydrogen bonds forming on GSH. They increase the tendency of the capped nanoparticles to bond with water and make them more suitable for use in the body [20]. Since lipids are kept on the surface at most GSH concentrations, this means capping does not remove necessary properties, but rather adds them to a more active exterior [7]. In brief, increased GSH levels lead to forming and intensifying specific GSH peaks (N–H, C=O, COO^-) without changing the intensity of the Zn–O and Fe–O bond vibrations. The results indicate that glutathione is bonded to the surface of the nanoparticles with its thiol and carboxylate parts, which helps in structural stability and colloidal control. The results match the findings of [45], who noticed the same change in wavelength when GSH was used to coat gold nanoparticles. Similarly, [46] found that GSH treatment of ZnO-based materials improved surface functional

groups and made them more stable, further proving their suitability for bioimaging. For bioimaging, it is greatly beneficial that the GSH-capped Fe: ZnO NPs have amine, carboxyl, and hydroxyl groups on their outer layer because they enable easy conjugation with biomolecules, thus making them fit for targeted imaging [47].

3. Conclusions

Herein, the effects of adding glutathione (GSH) to Fe: ZnO NPs and how it affects their structure, appearance, and suitability for bioimaging were studied. The XRD analysis confirmed that all samples had the hexagonal wurtzite structure of ZnO. $Fe^{3+}$was incorporated without the introduction of any secondary phases, and GSH capping decreased the crystallite size to 15.9 nm at 0.008M, which presents advantages for nanomedicine applications because of enhanced surface area and improved dispersibility. The PL analysis indicated that GSH capping led to enhanced emission intensity, with the effect being most notable at 0.008M concentration, because GSH reduced non-radiative recombination and facilitated light emission. Further examination of the spectra confirmed the presence of both near-band-edge and deep-level emissions, which were influenced by the GSH molecules on the NPs. The optical analysis revealed that the band gap decreased from 4.14 eV in uncapped Fe:ZnO to 3.0 eV with 0.008 M GSH due to more defects and changes in surface chemistry. FTIR analysis revealed that glutathione capping to the Fe-doped ZnO NPs occurred through N–H, C=O, and COO^- bonds.Therefore, using 0.008 M GSH as the capping agent gives the particles the right structure, a more compact size, more visible fluorescence, and a narrowband gap for optimum bioimaging outcomes. This confirms that the usage of GSH for surface engineering enhances the optical properties of Fe: ZnO NPs making them suitable for use in advanced medical imaging devices.

ACKNOWLEDGEMENTS

The authors wish to thank Murang'a University of Technology for offering access to various synthesis and characterization techniques for this research.

Conflict of Interest

The authors declare no conflict of interest.

REFERENCES

[1] A. B. Djurišić, X. Chen, Y. H. Leung, and A. Man Ching Ng, "ZnO nanostructures: growth, properties and applications," *J. Mater. Chem.*, vol. 22, no. 14, p. 6526, 2012, doi: 10.1039/c2jm15548f.

[2] V. Mariyappillai*et al.*, "Zr-modified ZnO nanoparticles: Optimized photocatalytic degradation and antibacterial efficiency for pollution control," *Ceram. Int.*, p. S0272884225010983, Feb. 2025, doi: 10.1016/j.ceramint.2025.02.402.

[3] J. Rosowska, J. Kaszewski, B. Witkowski, Ł. Wachnicki, I. Kuryliszyn-Kudelska, and M. Godlewski, "The effect of iron content on properties of ZnO nanoparticles prepared by microwave hydrothermal method," *Opt. Mater.*, vol. 109, p. 110089, Nov. 2020, doi: 10.1016/j.optmat.2020.110089.

[4] M. Carofiglio, S. Barui, V. Cauda, and M. Laurenti, "Doped Zinc Oxide Nanoparticles: Synthesis, Characterization and Potential Use in Nanomedicine," *Appl. Sci.*, vol. 10, no. 15, p. 5194, Jul. 2020, doi: 10.3390/app10155194.

[5] L. Guerrini, R. A. Alvarez-Puebla, and N. Pazos-Perez, "Surface Modifications of Nanoparticles for Stability in Biological Fluids," *Materials*, vol. 11, no. 7, p. 1154, Jul. 2018, doi: 10.3390/ma11071154.

[6] R. Javed, M. Usman, S. Tabassum, and M. Zia, "Effect of capping agents: Structural, optical and biological properties of ZnO nanoparticles," *Appl. Surf. Sci.*, vol. 386, pp. 319–326, Nov. 2016, doi: 10.1016/j.apsusc.2016.06.042.

[7] Z. Yang *et al.*, "Glutathione: a naturally occurring tripeptide for functional metal nanomaterials," *Chem. Sci.*, vol. 16, no. 16, pp. 6542–6572, 2025, doi: 10.1039/D4SC08599J.

[8] A. M. Alkilany and C. J. Murphy, "Toxicity and cellular uptake of gold nanoparticles: what we have learned so far?," *J. Nanoparticle Res.*, vol. 12, no. 7, pp. 2313–2333, Sep. 2010, doi: 10.1007/s11051-010-9911-8.

[9] C. Fernández-Ponce *et al.*, "Superficial Characteristics and Functionalization Effectiveness of Non-Toxic Glutathione-Capped Magnetic, Fluorescent, Metallic and Hybrid Nanoparticles for Biomedical Applications," *Metals*, vol. 11, no. 3, p. 383, Feb. 2021, doi: 10.3390/met11030383.

[10] S. Kumar *et al.*, "Effect of glutathione capping on the antibacterial activity of tin doped ZnO nanoparticles," *Phys. Scr.*, vol. 96, no. 12, p. 125807, Aug. 2021, doi: 10.1088/1402-4896/ac1eb3.

[11] Kavita, K. Singh, S. Kumar, and H. S. Bhatti, "Glutathione-assisted synthesis of star-shaped zinc oxide nanostructures and their photoluminescence behavior," *J. Lumin.*, vol. 149, pp. 112–117, May 2014, doi: 10.1016/j.jlumin.2014.01.001.

[12] M. Foyshal, M. F. Kabir, A. Islam, J. Ferdousy, M. R. Islam, and M. M. Rahman, "Enhanced Biocompatibility and Multifunctional Properties of Iron-Doped Zinc Oxide Nanoparticles for Applications," Oct. 18, 2023. doi: 10.21203/rs.3.rs-3426239/v1.

[13] A. C. Pierre, *Introduction to Sol-Gel Processing*. Cham: Springer International Publishing, 2020. doi: 10.1007/978-3-030-38144-8.

[14] A. Vishwakarma, "Synthesis of Zinc Oxide Nanoparticle by Sol-Gel Method and Study its Characterization," *Int. J. Res. Appl. Sci. Eng. Technol.*, vol. 8, no. 4, pp. 1625–1627, Apr. 2020, doi: 10.22214/ijraset.2020.4265.

[15] C.-Y. Tsay and T.-T. Huang, "Improvement of physical properties of IGZO thin films prepared by excimer laser annealing of sol–gel derived precursor films," *Mater. Chem. Phys.*, vol. 140, no. 1, pp. 365–372, Jun. 2013, doi: 10.1016/j.matchemphys.2013.03.051.

[16] Department of Physical and Biological Sciences, Murang'a University of Technology, PO BOX 75, Murang'a 10200, Kenya and J. Jepngetich, "Effects of Ag Doping Concentrations on Structural and Optical Properties of Citrus Reticulata Capped ZnO Nanoparticles," *J. Nanosci. Res. Rep.*, pp. 1–7, Apr. 2025, doi: 10.47363/JNSRR/2025(7)176.

[17] M. Alagiri, C. Muthamizhchelvan, and S. Ponnusamy, "Structural and magnetic properties of iron, cobalt and nickel nanoparticles," *Synth. Met.*, vol. 161, no. 15–16, pp. 1776–1780, Aug. 2011, doi: 10.1016/j.synthmet.2011.05.030.

[18] P. K. Sharma, R. K. Dutta, A. C. Pandey, S. Layek, and H. C. Verma, "Effect of iron doping concentration on magnetic properties of ZnO nanoparticles," *J. Magn. Magn. Mater.*, vol. 321, no. 17, pp. 2587–2591, Sep. 2009, doi: 10.1016/j.jmmm.2009.03.043.

[19] E. Moaseri*et al.*, "Reversible Self-Assembly of Glutathione-Coated Gold Nanoparticle Clusters via pH-Tunable Interactions," *Langmuir*, vol. 33, no. 43, pp. 12244–12253, Oct. 2017, doi: 10.1021/acs.langmuir.7b02446.

[20] R. Iyer *et al.*, "Glutathione-responsive biodegradable polyurethane nanoparticles for lung cancer treatment," *J. Controlled Release*, vol. 321, pp. 363–371, May 2020, doi: 10.1016/j.jconrel.2020.02.021.

[21] V. Mote, Y. Purushotham, and B. Dole, "Williamson-Hall analysis in estimation of lattice strain in nanometer-sized ZnO particles," *J. Theor. Appl. Phys.*, vol. 6, no. 1, p. 6, Dec. 2012, doi: 10.1186/2251-7235-6-6.

[22] A. Singh *et al.*, "Bandgap Modulation in ZnO Through Doping By Sol-Gel Method," presented at the SOLID STATE PHYSICS, PROCEEDINGS OF THE 55TH DAE SOLID STATE PHYSICS SYMPOSIUM 2010, Manipal, (India), 2011, pp. 595–596. doi: 10.1063/1.3605998.

[23] R. Jeyachitra, V. Senthilnathan, and T. S. Senthil, "Studies on electrical behavior of Fe doped ZnO nanoparticles prepared via co-precipitation approach for photo-catalytic application," *J. Mater. Sci. Mater. Electron.*, vol. 29, no. 2, pp. 1189–1197, Jan. 2018, doi: 10.1007/s10854-017-8021-0.

[24] P. Jamdagni, P. Khatri, and J. S. Rana, "Green synthesis of zinc oxide nanoparticles using flower extract of Nyctanthes arbor-tristis and their antifungal activity," *J. King Saud Univ. - Sci.*, vol. 30, no. 2, pp. 168–175, Apr. 2018, doi: 10.1016/j.jksus.2016.10.002.

[25] F. Sarf and H. Kızıl, "Defect Emission Energy and Particle Size Effects in Fe:ZnO Nanospheres Used in Li-Ion Batteries as Anode," *J. Electron. Mater.*, vol. 50, no. 11, pp. 6475–6481, Nov. 2021, doi: 10.1007/s11664-021-09191-1.

[26] D. Verma, A. K. Kole, and P. Kumbhakar, "Red shift of the band-edge photoluminescence emission and effects of annealing and capping agent on structural and optical properties of ZnO nanoparticles," *J. Alloys Compd.*, vol. 625, pp. 122–130, Mar. 2015, doi: 10.1016/j.jallcom.2014.11.102.

[27] Ma. D. L. Ruiz Peralta, U. Pal, and R. S. Zeferino, "Photoluminescence (PL) Quenching and Enhanced Photocatalytic Activity of Au-Decorated ZnO Nanorods Fabricated through Microwave-Assisted Chemical Synthesis," *ACS Appl. Mater. Interfaces*, vol. 4, no. 9, pp. 4807–4816, Sep. 2012, doi: 10.1021/am301155u.

[28] Y. Sun, W. Zhang, Q. Li, H. Liu, and X. Wang, "Preparations and applications of zinc oxide based photocatalytic materials," *Adv. Sens. Energy Mater.*, vol. 2, no. 3, p. 100069, Sep. 2023, doi: 10.1016/j.asems.2023.100069.

[29] P. Sikam, P. Moontragoon, J. Jumpatam, S. Pinitsoontorn, P. Thongbai, and T. Kamwanna, "Structural, Optical, Electronic and Magnetic Properties of Fe-Doped ZnO Nanoparticles Synthesized by Combustion Method and First-Principle Calculation," *J. Supercond. Nov. Magn.*, vol. 29, no. 12, pp. 3155–3166, Dec. 2016, doi: 10.1007/s10948-016-3690-0.

[30] A. Sandmann, A. Kompch, V. Mackert, C. H. Liebscher, and M. Winterer, "Interaction of L -Cysteine with ZnO: Structure, Surface Chemistry, and Optical Properties," *Langmuir*, vol. 31, no. 21, pp. 5701–5711, Jun. 2015, doi: 10.1021/la504968m.

[31] Q. Fan, X. Cui, H. Guo, Y. Xu, G. Zhang, and B. Peng, "Application of rare earth-doped nanoparticles in biological imaging and tumor treatment," *J. Biomater. Appl.*, vol. 35, no. 2, pp. 237–263, Aug. 2020, doi: 10.1177/0885328220924540.

[32] N. Madkhali, "Analysis of Structural, Optical, and Magnetic Properties of (Fe,Co) Co-Doped ZnO Nanoparticles Synthesized under UV Light," *Condens. Matter*, vol. 7, no. 4, p. 63, Nov. 2022, doi: 10.3390/condmat7040063.

[33] X. Yu *et al.*, "Enhanced photocatalytic activity of Fe-doped ZnO nanoparticles synthesized via a two-step sol–gel method," *J. Mater. Sci. Mater. Electron.*, vol. 25, no. 9, pp. 3920–3923, Sep. 2014, doi: 10.1007/s10854-014-2107-8.

[34] B. Choudhury, S. Bayan, A. Choudhury, and P. Chakraborty, "Narrowing of band gap and effective charge carrier separation in oxygen deficient TiO 2 nanotubes with improved visible light photocatalytic activity," *J. Colloid Interface Sci.*, vol. 465, pp. 1–10, Mar. 2016, doi: 10.1016/j.jcis.2015.11.050.

[35] C. Liu, Y. Ding, Q. Li, and Y. Lin, "Photochemical synthesis of glutathione-stabilized silver nanoclusters for fluorometric determination of hydrogen peroxide," *Microchim. Acta*, vol. 184, no. 7, pp. 2497–2503, Jul. 2017, doi: 10.1007/s00604-017-2302-4.

[36] L. Rulíšek and Z. Havlas, "Theoretical Studies of Metal Ion Selectivity. 1. DFT Calculations of Interaction Energies of Amino Acid Side Chains with Selected Transition Metal Ions (Co^{2+}, Ni^{2+}, Cu^{2+}, Zn^{2+}, Cd^{2+}, and Hg^{2+})," *J. Am. Chem. Soc.*, vol. 122, no. 42, pp. 10428–10439, Oct. 2000, doi: 10.1021/ja001265g.

[37] T. Janek, K. Sałek, J. Burger, Ż. Czyżnikowska, and S. R. Euston, "Investigating the biomolecular interactions between model proteins and glycine betaine surfactant with reference to the stabilization of emulsions and antimicrobial properties," *Colloids Surf. B Biointerfaces*, vol. 194, p. 111226, Oct. 2020, doi: 10.1016/j.colsurfb.2020.111226.

[38] S. Munir, S. M. Shah, H. Hussain, and R. Ali Khan, "Effect of carrier concentration on the optical band gap of TiO2 nanoparticles," *Mater. Des.*, vol. 92, pp. 64–72, Feb. 2016, doi: 10.1016/j.matdes.2015.12.022.

[39] M. Julita, M. Shiddiq, and M. Khair, "Determination of Band Gap Energy of ZnO/Au Nanoparticles Resulting in Laser Ablation in Liquid," *Indo J Chem Res*, vol. 10, no. 2, pp. 83–87, Sep. 2022, doi: 10.30598//ijcr.2022.10-mar.

[40] Y. Zheng, S. Gao, and J. Y. Ying, "Synthesis and Cell-Imaging Applications of Glutathione-Capped CdTe Quantum Dots," *Adv. Mater.*, vol. 19, no. 3, pp. 376–380, Feb. 2007, doi: 10.1002/adma.200600342.

[41] A. G. Kaninginiet *al.*, "Effect of Optimized Precursor Concentration, Temperature, and Doping on Optical Properties of ZnO Nanoparticles Synthesized via a Green Route Using Bush Tea (*Athrixiaphylicoides* DC.) Leaf Extracts," *ACS Omega*, vol. 7, no. 36, pp. 31658–31666, Sep. 2022, doi: 10.1021/acsomega.2c00530.

[42] W. Qi, Y. Tian, D. Lu, and B. Chen, "Detection of glutathione in dairy products based on surface-enhanced infrared absorption spectroscopy of silver nanoparticles," *Front. Nutr.*, vol. 9, p. 982228, Aug. 2022, doi: 10.3389/fnut.2022.982228.

[43] J. Andrade, C. G. Pereira, T. Ranquine, C. A. Azarias, M. J. V. Bell, and V. De Carvalho Dos Anjos, "Long-Term Ripening Evaluation of Ewes' Cheeses by Fourier-Transformed Infrared Spectroscopy under Real Industrial Conditions," *J. Spectrosc.*, vol. 2018, pp. 1–9, 2018, doi: 10.1155/2018/1381864.

[44] J.-J. Max and C. Chapados, "Infrared Spectroscopy of Aqueous Carboxylic Acids: Malic Acid," *J. Phys. Chem. A*, vol. 106, no. 27, pp. 6452–6461, Jul. 2002, doi: 10.1021/jp014377i.

[45] C. Battocchioet *al.*, "Gold Nanoparticles Stabilized with Aromatic Thiols: Interaction at the Molecule–Metal Interface and Ligand Arrangement in the Molecular Shell Investigated by SR-XPS and NEXAFS," *J. Phys. Chem. C*, vol. 118, no. 15, pp. 8159–8168, Apr. 2014, doi: 10.1021/jp4126057.

[46] T. D. Kusworo, F. Dalanta, N. Aryanti, and N. H. Othman, "Intensifying separation and antifouling performance of PSf membrane incorporated by GO and ZnO nanoparticles for petroleum refinery wastewater treatment," *J. Water Process Eng.*, vol. 41, p. 102030, Jun. 2021, doi: 10.1016/j.jwpe.2021.102030.

[47] S. V. Kaymaz, H. M. Nobar, H. Sarıgül, C. Soylukan, L. Akyüz, and M. Yüce, "Nanomaterial surface modification toolkit: Principles, components, recipes, and applications," *Adv. Colloid Interface Sci.*, vol. 322, p. 103035, Dec. 2023, doi: 10.1016/j.cis.2023.103035.